Journal of Innate Immunity

Research Article

J Innate Immun 2023;15:562–580
DOI: 10.1159/000530374

Received: October 13, 2022
Accepted: March 3, 2023
Published online: March 25, 2023

Impact of Changes in Human Airway Epithelial Cellular Composition and Differentiation on SARS-CoV-2 Infection Biology

Melissa Thaler[a] Ying Wang[b] Anne M. van der Does[b] Alen Faiz[c] Dennis K. Ninaber[b] Natacha S. Ogando[a] Hendrik Beckert[d] Christian Taube[d] Clarisse Salgado-Benvindo[a] Eric J. Snijder[a] Peter J. Bredenbeek[a] Pieter S. Hiemstra[b] Martijn J. van Hemert[a]

[a]Department of Medical Microbiology, Leiden University Medical Center, Leiden, The Netherlands; [b]Department of Pulmonology, Leiden University Medical Center, Leiden, The Netherlands; [c]Respiratory Bioinformatics and Molecular Biology (RBMB), School of Life Sciences, University of Technology Sydney, Sydney, NSW, Australia; [d]Department of Pulmonary Medicine, University Medical Center Essen – Ruhrlandklinik, Essen, Germany

Keywords
SARS-CoV-2 · Human airway epithelial cells · Infection biology · Cellular composition · Cell culture

Abstract
The consequences of infection with severe acute respiratory syndrome coronavirus 2 (SARS-CoV-2) can range from asymptomatic to fatal disease. Variations in epithelial susceptibility to SARS-CoV-2 infection depend on the anatomical location from the proximal to distal respiratory tract. However, the cellular biology underlying these variations is not completely understood. Thus, air-liquid interface cultures of well-differentiated primary human tracheal and bronchial epithelial cells were employed to study the impact of epithelial cellular composition and differentiation on SARS-CoV-2 infection by transcriptional (RNA sequencing) and immunofluorescent analyses. Changes of cellular composition were investigated by varying time of differentiation or by using specific compounds. We found that SARS-CoV-2 primarily infected not only ciliated cells but also goblet cells and transient secretory cells. Viral replication was impacted by differences in cellular composition, which depended on culturing time and anatomical origin. A higher percentage of ciliated cells correlated with a higher viral load. However, DAPT treatment, which increased the number of ciliated cells and reduced goblet cells, decreased viral load, indicating the contribution of goblet cells to infection. Cell entry factors, especially cathepsin L and transmembrane protease serine 2, were also affected by differentiation time. In conclusion, our study demonstrates that viral replication is affected by changes in cellular composition, especially in cells related to the mucociliary system. This could explain in part the variable susceptibility to SARS-CoV-2 infection between individuals and between anatomical locations in the respiratory tract.

Pieter S. Hiemstra and Martijn J. van Hemert contributed equally to this work.
Melissa Thaler and Ying Wang share first authorship.

karger@karger.com
www.karger.com/jin

Correspondence to:
Pieter S. Hiemstra, P.S.Hiemstra@lumc.nl
Martijn J. van Hemert, M.J.van_Hemert@lumc.nl

Introduction

Since December 2019, severe acute respiratory syndrome coronavirus 2 (SARS-CoV-2) has rapidly spread worldwide. The burden of the associated disease COVID-19 has an enormous medical, social, and economic impact [1]. Furthermore, the continuing emergence of virus variants, such as the delta and omicron variants, is associated with additional waves of COVID-19 cases [2, 3]. This illustrates the threat of these viruses to prolong the current pandemic or lead to new large outbreaks in the future. Besides different clinical outcomes due to SARS-CoV-2 variants, even people infected with the same virus variant present with varying clinical signs and symptoms depending on age [4], sex [5], weight [6], environment [7], other medical conditions [6, 8], immune status [9], and possibly other yet-to-be-identified factors.

SARS-CoV-2 was first isolated from the lower respiratory tract of COVID-19 patients [10, 11]. The epithelium serves as the first barrier to SARS-CoV-2 infection in the respiratory tract, and therefore, the subsequent epithelial response to infection (antiviral and inflammatory responses) plays an important role in the outcome of infection. The respiratory tract spans from the nasal cavity to the terminal bronchioles, ending in the alveoli where gas exchange occurs. The airways are lined by the airway epithelium, which includes various cell types, of which ciliated, secretory goblet, and club cells and basal cells are present in the highest numbers [12, 13]. These cell types have their own distinct functions. For instance, goblet cells secrete mucus, which captures inhaled particles like respiratory viruses, while the continuous beating cilia from ciliated cells help to transport this mucus with entrapped particles toward the pharynx, collectively called mucociliary clearance (MCC). Although the airway epithelium shares similar cell types throughout the respiratory tract, the proportion of each cell type is dependent on the anatomical location [13]. In addition, in many patients with lung diseases such as asthma or chronic obstructive pulmonary disease, epithelial cellular composition is altered [12]. In primary airway epithelial cell cultures, which are differentiated at the air-liquid interface (ALI), cellular composition of the airway epithelium depends on the individual donor [14], differentiation time [15], and culture conditions [16]. So far, the impact of epithelial cellular composition on SARS-CoV-2 infection biology has not been completely elucidated. Previous studies have demonstrated a difference in host susceptibility to SARS-CoV-2 infection depending on the location of virus-host interaction in the respiratory tract [17]. However, it is unclear to what extent the differences in viral replication link to variation in epithelial cellular composition. SARS-CoV-2 targets ciliated and secretory cells [18, 19], possibly via strands of mucus attached to cilia tips [20]. Therefore, changes in the proportion of these target cells might affect viral replication. SARS-CoV-2 cellular tropism furthermore depends on host proteins that are involved in virus entry, including angiotensin-converting enzyme 2 (ACE2) and proteases like transmembrane protease serine 2 (TMPRSS2) and cathepsin L (CTSL), as well as alternative receptors (e.g., cluster of differentiation 147 [CD147], 78-kDa glucose-regulated protein [GRP78], tyrosine-protein kinase receptor UFO [AXL]), which all have been demonstrated to be expressed in variable levels on human airway epithelial cells [21–24]. Recent research demonstrated that SARS-CoV-2 cell entry factors are primarily expressed in bronchial transient secretory cells [25], indicating these transiently differentiating cells might contribute to a great extent to initial infection.

While research on the susceptibility of respiratory epithelial cells to SARS-CoV-2 infection often focuses on a specific cell type, function, or protein of interest [26], we aimed to investigate how various changes in cellular differentiation and composition affect SARS-CoV-2 infection biology. This knowledge can support our understanding of how these factors could contribute to local, and – more importantly – airway disease-associated differences in susceptibility. To this end, we used primary human bronchial (PBEC) and tracheal epithelial cells (PTEC) and differentiated them at the ALI for up to 5 weeks. We characterized virus replication, spread, localization, immune responses, and expression of SARS-CoV-2-entry factors, as well as compared cellular composition between both types of cultures. Furthermore, we investigated how infection characteristics were influenced by modulation of the cellular composition and by the duration of culture.

Materials and Methods

Cell Culture

PBEC were isolated from tumor-free resected bronchial tissue that was obtained from patients undergoing resection surgery for lung cancer at the Leiden University Medical Center (Leiden, The Netherlands). Patients from whom this PBEC were derived were enrolled in the biobank via a no-objection system for coded anonymous further use of such tissue (www.coreon.org). However, since January 9, 2022, patients have been enrolled in the biobank using active informed consent in accordance with local regulations from the LUMC Biobank with approval from the Institutional

Medical Ethical Committee (B20.042/Ab/ab and B20.042/Kb/kb). PTEC were isolated from residual tracheal and main stem bronchial tissue from lung transplant donors postmortem at the University Medical Center Essen (Essen, Germany). Use of such donor tissue for research was approved by the Ethical Committee of the medical faculty of the University of Duisburg-Essen (ID: 19-8717-BO) [27].

To achieve mucociliary differentiation, PBEC and PTEC were cultured at the ALI as previously described [28]. Briefly, epithelial cell cultures from individual donors or mixed donors were seeded onto 12-insert Transwell membranes (Corning Costar, Cambridge, MA, USA), which were coated with PBS supplemented with 5 μg/mL human fibronectin (Promocell, Heidelberg, Germany), 30 μg/mL PureCol (Advanced BioMatrix, CA, USA), and 10 μg/mL bovine serum albumin (Fraction V; Thermo Fisher Scientific, Carlsbad, CA, USA), in a 1:1 mixture of Bronchial Epithelial Cell Medium-basal (ScienCell, SanBio) and Dulbecco's Modified Eagle's Medium (STEMCELL Technologies, Köln, Germany), further referred to as B/D medium. This B/D medium contains 12.5 mM HEPES, bronchial epithelial cell growth supplement, 100 U/mL penicillin, 100 μg/mL streptomycin (all from ScienCell), 2 mM GlutaMAX (Thermo Fisher Scientific). B/D medium was supplemented during submerged culture with 1 nM EC23 (light-stable retinoic acid receptor agonist; Tocris, Abingdon, UK). For individual donors, the seeding intensity was 40,000 cells/12-insert and for mixed donors approximately 150,000 cells (30,000 cells/donor when mixing cells from 5 donors and 40,000 cells/donor when using 4 donors). For the donor mixes, the higher seeding density compared to individual cultures resulted in near-confluency to avoid selective advantage of possible faster proliferating cells of specific donors.

After confluency was reached, the apical medium was removed and cells were cultured at the ALI in B/D medium with 50 nM EC23 for 3–5 weeks; during this period, medium was refreshed, and the apical side was washed three times a week with warm PBS to remove excess mucus. To shift cell differentiation toward an increased number of goblet or ciliated cells, ALI-PBEC were incubated in BD medium supplemented with 50 nM EC23, and either 1 ng/mL IL-13 (PeproTech) or 5 μM DAPT (γ-secretase inhibitor, Tocris) from day 22 to day 35 culture time. To assess the direct effect of DAPT, we treated cells with DAPT either starting 24 h before (and during) infection (a time period considered insufficient to cause a shift in epithelial differentiation) or directly after infection.

Vero E6 cells (master stock MM-3 from the Dept. of Medical Microbiology collection, characterized by full-genome sequencing) were maintained in Dulbecco's Modified Eagle's Medium with 4.5 g/L glucose with L-glutamine (Lonza), supplemented with 8% fetal calf serum (Capricorn Scientific) and 100 U/mL of penicillin/streptomycin (Sigma-Aldrich). All cell cultures were maintained at 37°C. Infections for plaque assays in Vero E6 cells were performed in Eagle's Minimal Essential Medium with 25 mM HEPES (Lonza) supplemented with 2% FCS, 2 mM L-glutamine (Sigma-Aldrich), and 100 U/mL of penicillin/streptomycin (Sigma-Aldrich).

SARS-CoV-2 Virus

The clinical isolate SARS-CoV-2/Leiden-0002 was isolated from a nasopharyngeal sample collected at the LUMC (GenBank accession nr. MT510999). The virus was passaged twice in Vero E6 cells to obtain the virus stock used for infection. Virus titers were determined by plaque assay as described before [29]. All experiments with infectious SARS-CoV-2 were performed at the Leiden University Medical Center biosafety level 3 facilities.

SARS-CoV-2 Infection of ALI-PBEC

Prior to infection, the mucus was removed by washing the apical surface of the ALI cultures with 200 μL PBS and aspirating it after a 10-min incubation at 37°C. Basal medium was changed every 2 days. Cells were infected with 200 μL of inoculum prepared in PBS, containing 30,000 PFU of SARS-CoV-2 per insert for 2 h at 37°C on a rocking platform (estimated multiplicity of infection [MOI] of 0.03). PBS was used as the solvent control and in mock-infected cells as the inoculum. After removal of the inoculum, the apical side was washed three times with PBS, and cells were incubated at 37°C. Viral progeny was harvested from the apical side at 24, 48, and 72 hpi as described in the next section.

Cells were infected after 3–5 weeks of differentiation as indicated. For cells under DAPT or IL-13 treatment, the medium was supplemented with 1 ng/mL IL-13 or 5 μM DAPT after 3 weeks of differentiation, and after 5-week culture time in total (2 weeks of treatment), PBEC were infected. After infection, the basal medium was replaced by fresh B/D medium also supplemented with IL-13 or DAPT.

RNA Isolation, Quantitative RT-PCR/Real-Time PCR, and Plaque Assay Analysis

Apical washes were harvested following a 10-min incubation at 37°C with 200 μL PBS. RNA was isolated from half the volume of apical washes (100 μL) after addition of 800 μL of TriPure Isolation Reagent (Sigma-Aldrich). TriPure reagent was spiked with equine arteritis virus to control for variation in RNA extraction efficiency and possible inhibitors of real-time PCR (RT-qPCR). Intracellular RNA was isolated by adding 500 μL of TriPure reagent directly to cells on the insert. Samples were stored at −20°C until RNA was isolated using the Direct-zol™-96 RNA plate isolation (Zymo), 5PRIME Phase Lock Gel extraction (Quantabio) or Maxwell® 16 simply RNA tissue kit (Promega, the Netherlands). The phosphoglycerate kinase 1 (*PGK-1*) was used as a reference gene for normalization when intracellular RNA was analyzed. Primers and probes for equine arteritis virus and *PGK-1* (Sigma-Aldrich) and the normalization procedure were performed as described before [29]. Viral RNA was quantified by internally controlled multiplex RT-qPCR using the TaqMan™ Fast Virus 1-Step Master Mix (Thermo Fisher Scientific) as described previously [30] but with modifications as listed in Table 1. A standard curve generated by RT-qPCR on 10-fold serial dilutions of a T7 RNA polymerase-generated in vitro transcript containing the target sequences was used for absolute quantification of RNA copy numbers.

For analysis of the transcriptional response of epithelial cells to infection, RNA was reverse-transcribed and cDNA was amplified by real-time qPCR (Bio-Rad, Veenendaal, The Netherlands) using specific primers. Relative normalized gene expression compared to reference genes ribosomal protein L13a (RPL13A) and ATP synthase, H^+-transporting, mitochondrial F1 complex, beta polypeptide (ATP5B) was calculated according to the standard curve method. Reference genes were selected out of 8 candidate reference genes using the "Genorm" software (Genorm; Primer Design, Southampton, UK). RT-qPCR was performed on a CFX384 Touch™ Real-Time PCR Detection System (Bio-Rad) using a program consisting of 5 min at 50°C and 20 s at 95°C (or

Table 1. Primer sequences

Gene	Forward primer (5′-3′)	Reverse primer (5′-3′)
E	ACAGGTACGTTAATAGTTAATAGCGT	ATATTGCAGCAGTACGCACACA
E probe	TexRed-ACACTAGCCATCCTTACTGCGCTTCG-BHQ1	
RdRp	GTGARATGGTCATGTGTGGCGG	CARATGTTAAASACACTATTAGCATA
RdRp probe	FAM-CAGGTGGAACCTCATCAGGAGATGC-BHQ1	
MUC5AC	CCTTCGACGGACAGAGCTAC	TCTCGGTGACAACACGAAAG
FOXJ1	GGAGGGGACGTAAATCCCTA	TTGGTCCCAGTAGTTCCAGC
SCGB1A1	ACATGAGGGAGGCAGGGGCTC	ACTCAAAGCATGGCAGCGGCA
TP63	CCACCTGGACGTATTCCACTG	TCGAATCAAATGACTAGGAGGGG
IFNL1	GGACGCCTTGGAAGAGTCACT	AGAAGCCTCAGGTCCCAATTC
IFNB1	ATGACCAACAAGTGTCTCCTCC	GGAATCCAAGCAAGTTGTAGCTC
CXCL8	CTGGACCCCAAGGAAAAC	TGGCAACCCTACAACAGAC
IL6	CAGAGCTGTGCAGATGAGTAC A	GATGAGTTGTCATGTCCTGCA
ACE2	CGTCTGAATGACAACAGCCTAGA	AATGCCAACCACTATCACTCCC
TMPRSS2	AATCGGTGTGTTCGCCTCTAC	CGTAGTTCTCGTTCCAGTCGT
CD147	CAGAGTGAAGGCTGTGAAGTCG	TGCGAGGAACTCACGAAGAAC
GRP78	GGAAAGAAGGTTACCCATGC	AGAAGAGACACATCGAAGGT
ATP5B	TCACCCAGGCTGGTTCAGA	AGTGGCCAGGGTAGGCTGAT
RPL13A	AAGGTGGTGGTCGTACGCTGTG	CGGGAAGGGTTGGTGTTCATCC

3 min at 95°C when cDNA was used), followed by 45 cycles of 5 s at 95°C and 30 s at 60°C or 63°C (depending on primers). Primer pairs are listed in Table 1. For quantification of the number of infectious virus particles, the apical wash was serially diluted, and infectious titers were determined by plaque assay on Vero E6 as described previously [29].

Immunofluorescence Staining

For analysis by immunofluorescence, ALI cultures were rinsed using PBS and cells were fixed by adding 3% (w/v) paraformaldehyde diluted in PBS into the basal and apical compartments followed by incubation at room temperature for at least 35 min. Next, inserts were washed two times with PBS and stored in PBS with 10 mM glycine at 4°C until further use. Ice-cold methanol was added for 10 min at 4°C, and PBS containing 1% (w/v) BSA, 0.3% (w/v) Triton-X-100 was used to block nonspecific binding sites and permeabilize cells for 30 min at 4°C. Membranes were excised from the insert and cut into 4 pieces that were incubated overnight at 4°C with specific antibodies at the following dilutions: rabbit anti-SARS-CoV-2 N antibody (JUC3, 1:500 [31]), human anti-SARS-CoV-2 spike antibody (P008_076 [32]), mouse anti-MUC5AC antibody (1:200; Thermo Fisher Scientific), mouse anti-acetylated α-tubulin (1/100; Sigma-Aldrich), or goat anti-FOXJ1 antibody (1:200; R&D, Minneapolis, MN, USA). After washing, membranes were incubated with corresponding secondary antibodies: donkey anti-rabbit, donkey anti-mouse, or donkey anti-goat Alexa Fluor antibodies (all diluted 1:200, Thermo Fisher Scientific) and 4′,6-diamidino-2-phenylindole (DAPI, 1:200, Sigma-Aldrich) in the dark for 30 min at room temperature. Next, membranes were transferred to glass slides and covered with ProLong Gold Antifade reagent (Thermo Fisher Scientific) and a coverslip (VWR, Amsterdam, The Netherlands). Slides were viewed using a Leica TCS SP8 confocal microscope (Leica Microsystems, Wetzlar, Germany), the Andor Dragonfly 500 spinning disk confocal (Andor Technology, Belfast, UK), or the ZEISS Axio Scan.Z1 Slide Scanner (ZEISS, Oberkochen, Germany) at ×100/×400/×630 original magnification according to experimental requirements. Positive-stained cells from three random areas of each insert membrane of each independent experiment were quantified by ImageJ.

RNA Sequencing and Analysis

The samples harvested from 3-week and 5-week differentiated ALI-PBEC and ALI-PTEC were used to perform RNA sequencing (RNA-Seq) at GenomeScan (Leiden, The Netherlands). Total RNA was extracted using TriPure Isolation Reagent and the Maxwell® 16 simply RNA tissue kit and passed the quality control measured by the Fragment Analyzer. Then mRNA was isolated based on poly-A selection, and RNA fragmentation was performed. After that, cDNA was synthesized for adapter ligation and PCR amplification. A data set of 12 samples was generated using an Illumina NovaSeq 6000 sequencer, and the quality for the raw data was determined with third-party (FastQC v0.11.9) and in-house (FastQA v3.1.25) quality control tools. The paired-end reads were trimmed to remove possible adapter sequences using cutadapt v2.10 and mapped to the human GRCh37.75 (Homo_sapiens.GRCh37.75.dna.primary assembly.fa). Based on the mapped locations in the alignment file, the frequency of how often a read was mapped on a transcript was determined with HTSeq v0.11.0. RNA-Seq analysis was performed using the R package DeSeq2 with the read counts ≥10. Differential expression was conducted comparing virus infection at each time point to time matched no virus control/mock. Gene signatures were made using the Gene Set Variation Analysis package. The differentially expressed genes (DEGs) were generated by comparing data in 5-week cultures compared to 3-week cultures, and the significant differences were considered when they had a Benjamini-Hochberg p value <0.1 and a fold change >|2|. The gene sets of DEGs were further analyzed by gene set enrichment analysis using the website www.gsea-msigdb.org as previously reported [33, 34].

Cellular Deconvolution

The relative proportion of each cell type (ciliated, secretory, basal, and rare cells) was predicted using cellular deconvolution analysis of bulk RNA-Seq data as previously described [35]. To this end, genes were selected using AutoGeneS software on the Human Lung Cell Atlas v1.0 dataset [36] based on minimized correlation and maximized distance between clusters. After that, genes with the most stable results across cohorts were selected and used to deduce major cell type proportions. The RNA-Seq data were subsequently normalized to counts per million, and highly variable genes (N = 5,000) were selected. Next, on all samples, bulk deconvolution was performed using the CIBERSORT support vector regression method [37]. The relative proportion of cell types was compared between 3-week cultures and 5-week cultures from ALI-PBEC or ALI-PTEC using paired two-way ANOVA with Tukey's test.

Statistical Analysis

Statistical analysis was performed in GraphPad PRISM 9.0 (GraphPad Software Inc., La Jolla, CA). Differences were assessed by a paired one-way with Tukey's test, paired two-way ANOVA with Tukey's test, or paired two-tailed t test. Data were shown as mean values ± SEM, and differences were considered significant at $p < 0.05$.

Results

Susceptibility of Airway Epithelial Cultures to SARS-CoV-2 Differs between Individual Donors

To investigate the effect of differentiation status and cellular composition of the airway epithelium on SARS-CoV-2 infection biology, we first aimed to establish a reliable infection model. We investigated donor-dependent variability in infection by comparing SARS-CoV-2 replication kinetics in cultures of 4 individual donors and a mix of those donors. Between the single-donor cultures, we observed some variation in the viral load (Fig. 1a). Cultures derived from mixes of primary cells from these donors (donor mix) showed comparable infection kinetics with regard to this variation, and immunofluorescence staining confirmed similar numbers of infected cells at 72 h post infection (hpi) for single donors and donor mix (Fig. 1b). Thus, ALI-PBEC cultures of mixed donor cells proved to be a representative model to investigate characteristics of airway epithelial cell cultures and to test many variables, while keeping sample size relatively limited.

We performed infections at a relatively low MOI to model the initial stage of infection by initially only infecting a fraction of susceptible cells and observe the virus spread across the epithelium over time. Four independent experiments were performed using ALI-PBEC derived from the same donor mix. After infection with SARS-CoV-2 (30,000 PFU per insert), we observed an increase in the viral load (extracellular copies of viral RNA) over time, to approximately 10^{11} copies/mL at 72 hpi (Fig. 1c). Immunofluorescence staining of the epithelial cultures for viral nucleocapsid protein also showed a gradual increase in the number of infected cells over time (Fig. 1d). The number of infected cells was low and generally detected at the edge of the insert (online suppl. Fig. S1a; for all online suppl. material, see https://doi.org/10.1159/000530374) as also previously reported [38].

To validate the relevance of our cell culture model for studying epithelial defense against SARS-CoV-2 infection, we measured antiviral responses (IFN-β1 and IFN-λ1) and inflammatory cytokines (IL-6 and IL-8 [CXCL8]) (online suppl. Fig. S1). We observed that SARS-CoV-2 infection did not affect mRNA levels of *IFNB1* and *IFNL1* at 24 and 48 h but strongly increased their expression at 72 hpi (online suppl. Fig. S1b). At 72 hpi, mRNA levels of both *IL-6* and *CXCL8* displayed a modest but significant increase in SARS-CoV-2-infected cultures (online suppl. Fig. S1c). We established reproducible and robust infection kinetics in this model, accompanied by a significant but late epithelial antiviral and inflammatory response that is characteristic for SARS-CoV-2 infection [39].

SARS-CoV-2 Primarily Infects Epithelial Cells Involved in MCC

Previous studies have indicated that within the human respiratory tract, predominantly ciliated cells, but also goblet cells of the airway epithelium, can be infected with SARS-CoV-2 [19], as well as alveolar epithelial cells [40, 41]. To assess if ciliated and goblet cells were also the target cells in our cultures, we investigated the colocalization of SARS-CoV-2 nucleocapsid protein with either acetylated α-tubulin and FOXJ1 as markers for ciliated cells or MUC5AC as a marker for goblet cells. Recently, a new transient secretory cell subtype which is positive for markers of ciliated and goblet cells was suggested to be particularly susceptible to SARS-CoV-2 based on ACE2 and TMPRSS2 expression [25]. We observed the presence of most of the viral nucleocapsid protein in acetylated α-tubulin-positive ciliated cells in ALI-PBEC cultures, with less presence in $MUC5AC^+$ goblet cells (Fig. 1e), showing that both cell types can indeed be infected by SARS-CoV-2. Additionally, immunofluorescence staining showed that few transient secretory cells – defined as FOXJ1- and MUC5AC-double-positive cells – were present and infected by SARS-CoV-2 (Fig. 1f).

We next investigated if the number of SARS-CoV-2 target cells in the single-donor cultures depicted in

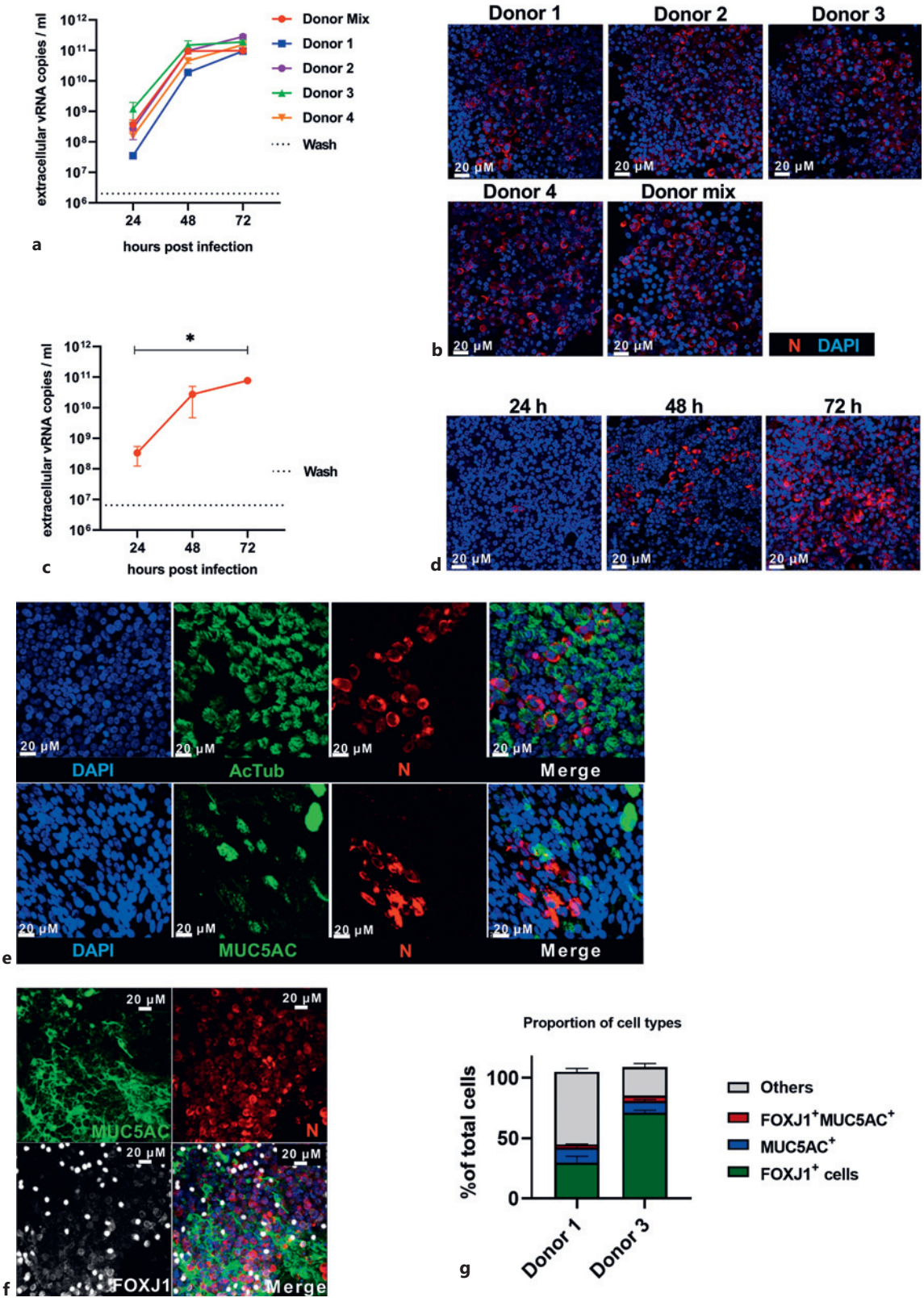

1

(For legend see next page.)

Figure 1a correlated with the level of infection. Interestingly, quantification by immunofluorescence staining showed that cultures from donor 3, which had the higher initial viral load (at 24 hpi) compared to cells from donor 1 with the lowest initial viral load, constituted a higher proportion of FOXJ1$^+$ ciliated cells, as well as transient secretory cells (Fig. 1g). This result suggests that the differences in susceptibility of cultures from different donors to viral infection might be associated with variation in the percentages of the different SARS-CoV-2 target cells.

Modulating Epithelial Cellular Composition Has Moderate Effects on SARS-CoV-2 Infection

To further explore the association between epithelial cellular composition and viral infection, we skewed cellular differentiation of ALI-PBEC during the last 2 weeks of differentiation to either an enrichment in ciliated cells at the cost of goblet cells or toward an enrichment in goblet cells at the expense of ciliated cells using DAPT or interleukin 13 (IL-13), respectively [28, 42, 43]. We infected these cultures with SARS-CoV-2 to analyze if enrichment in one of these cell types impacted infection kinetics. We could verify that DAPT treatment caused a marked increase in the number of ciliated cells (FOXJ1$^+$ and acetylated α-tubulin$^+$), while the number of goblet cells (MUC5AC$^+$) was decreased (Fig. 2a; online suppl. Fig. S2a). Conversely, IL-13 treatment increased the fraction of goblet cells and decreased the number of ciliated cells (Fig. 2a; online suppl. Fig. S2a), also confirmed at the gene expression level (online suppl. Fig. S2b). Additionally, a small percentage of FOXJ1- and MUC5AC-double-positive transient secretory cells was detected in all cultures, which was not significantly affected by IL-13 or DAPT treatment (online suppl. Fig. S2a).

We infected these DAPT- or IL-13-treated cultures with SARS-CoV-2 and in line with the data shown in Figure 1, detected by immunofluorescence staining that only a few cells were infected at 24 hpi in untreated and treated cultures (Fig. 2b). At 48 and 72 hpi, all cultures showed an increase in the viral load compared to 24 hpi (Fig. 2b), demonstrating that viral infection and replication were feasible in all cultures despite the significant change in cellular composition between these conditions. In IL-13-treated cell cultures, intracellular viral RNA levels were highest at 48 hpi, while being similar to control again at 72 hpi (Fig. 2c). To our surprise, the level of intracellular SARS-CoV-2 RNA was lower in DAPT-treated cells at all time points compared to the controls (Fig. 2c). Similar trends were found for the release of infectious particles, as shown in Figure 2d. When we checked for cell types infected with SARS-CoV-2 in DAPT-treated cultures, due to the lack of goblet cells, ciliated cells were the only identified cells. In IL-13-treated cultures, we observed infection of ciliated and goblet cells, similar to control cultures (Fig. 2e).

To exclude the possibility that the effects observed in DAPT-treated cultures were a direct consequence of inhibition of Notch signaling rather than epithelial remodeling, we treated cells with DAPT either starting 24 h before (and during) infection (a time period considered insufficient to cause a shift in epithelial differentiation) or directly after infection. These short-term treatments with DAPT did not result in significant changes in the intracellular viral RNA copies or production of infectious

Fig. 1. Characterization of a SARS-CoV-2 infection model using ALI cultures of primary bronchial epithelial cells. Mixes of PBEC derived from 4–5 individual donors were cultured for 5 weeks at ALI before they were infected with SARS-CoV-2 (30,000 PFU per insert). **a** Viral load in cultures derived from single donors or a mix of these donors (in red) was determined by quantifying the level of extracellular viral RNA copies by RT-qPCR. The dashed line represents the amount of (input) viral RNA that remained in the last wash after washing the inserts at 2 hpi (mean of all donors). **b** Infected cells were stained with rabbit polyclonal anti-SARS-CoV-2 N protein antibody (JUC3) and with 4′,6-diamidino-2-phenylindole (DAPI) and visualized by immunofluorescence microscopy at 72 hpi. Images shown at ×400 original magnification are representative merged z-stack images for results obtained with cells from random areas of the inserts. **c** Viral load at 24, 48, and 72 hpi in cultures was determined by quantifying the number of extracellular viral RNA copies by RT-qPCR. Data are mean ± SEM. $n = 4$ independent experiments with the same donor mix. **d** For immunofluorescence microscopy, cells were fixed at 72 hpi and (double-) labeled with rabbit polyclonal anti-SARS-CoV-2 N protein antibody (JUC3) and with DAPI for nuclear staining. Images shown at ×400 original magnification are representative merged z-stack images for results obtained with cells from 3 independent experiments. **e** Immunofluorescence staining at 72 hpi, with antibodies against acetylated α-tubulin (ciliated cell marker) or MUC5AC (goblet cell marker) in combination with anti-SARS-CoV-2 N protein antibody (JUC3) and DAPI for nuclear staining. Immunofluorescence images shown are representative merged z-stack images for results of 3 independent experiments with ×630 original magnification. **f** Immunofluorescence staining with antibodies against MUC5AC and FOXJ1 (ciliated cell marker) with anti-SARS-CoV-2 N protein antibody and DAPI for nuclear staining. Immunofluorescence images shown are representative merged z-stack images for results of 3 independent experiments with ×400 original magnification. **g** Quantification of immunostaining of FOXJ1$^+$, MUC5AC$^+$, and FOXJ1$^+$MUC5AC$^+$ or other cells in cultures of two single donors was performed with ImageJ software.

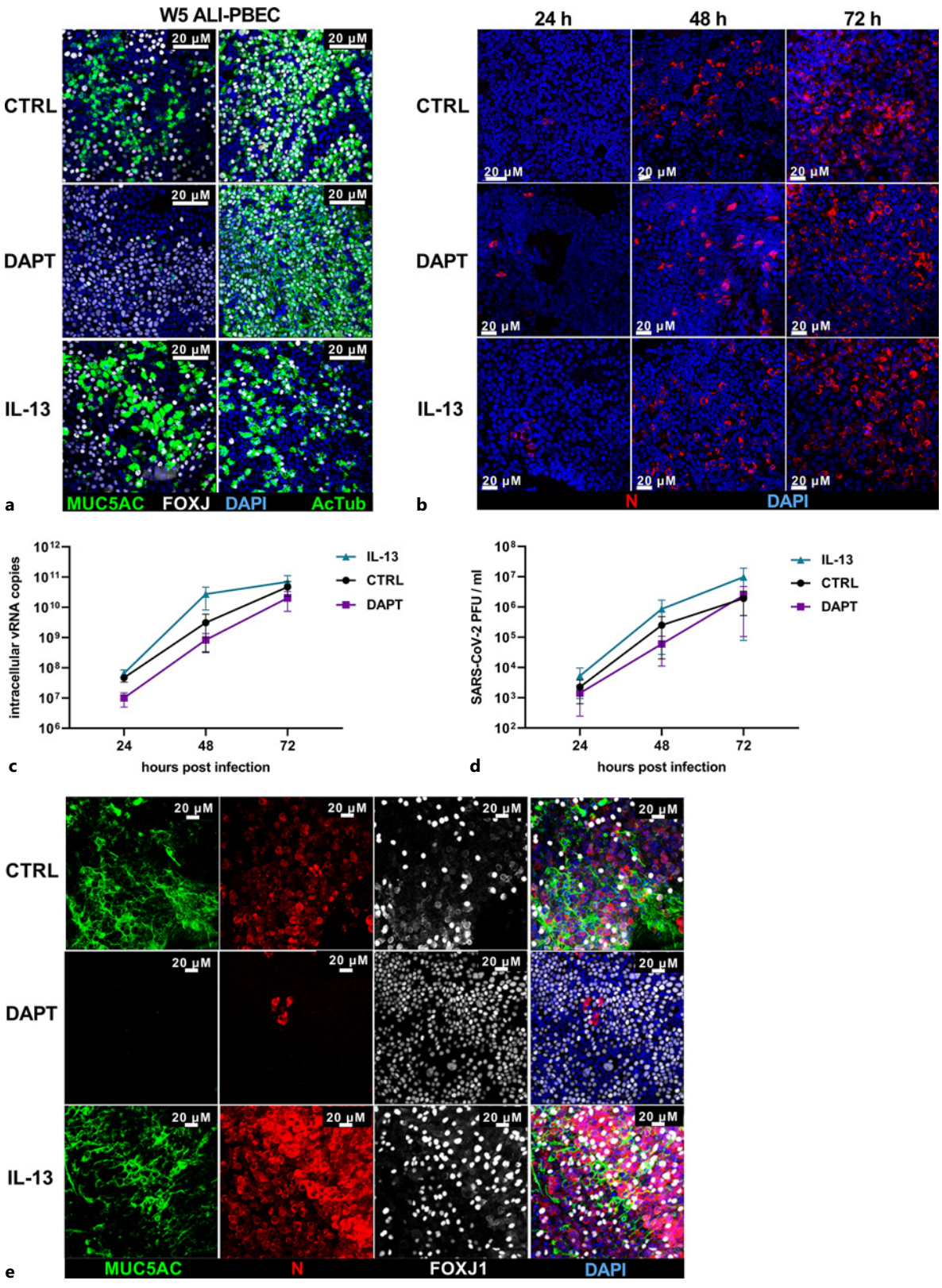

2

(For legend see next page.)

progeny, suggesting that inhibition of Notch signaling itself has no direct effect on SARS-CoV-2 replication (online suppl. Fig. S2c). These data suggest that rather than one cell type alone, possibly the interplay between goblet and ciliated cells is important for susceptibility of ALI-PBEC to SARS-CoV-2 infection.

Origin and Culture Duration of Human Airway Epithelial Cells Affect SARS-CoV-2 Infection

Next, we wanted to investigate how differentiation time and anatomical origin of the epithelial cultures affected SARS-CoV-2 infection biology. To this end, we employed cells isolated from bronchial or tracheal tissue and allowed ALI-PBEC and ALI-PTEC to differentiate for 3, 4, or 5 weeks, after which they were infected with 30,000 PFU of SARS-CoV-2. The viral load was analyzed at 72 hpi. In both ALI-PBEC and ALI-PTEC, an increase in intra- and extracellular viral RNA as well as infectious virus particles was observed with longer differentiation time, with the highest viral load observed in cultures differentiated for 5 weeks after start of ALI (Fig. 3a–c). A gradual 1–2 log increase in SARS-CoV-2 progeny production was observed when cultures had been differentiated up to 5 weeks when compared to 3 weeks of differentiation (online suppl. Fig. S3a). Immunofluorescence staining of these cultures for the viral nucleocapsid protein also demonstrated an increase in the number of infected cells with increasing culture duration (Fig. 3c). A significantly higher viral load was observed in ALI-PBEC compared to ALI-PTEC, with an average 10-fold difference in extracellular SARS-CoV-2 RNA copies (Fig. 3a, b) and infectious progeny (Fig. 3c), in particular, in 5-week differentiated cultures. In conclusion, our results show that both the anatomical origin of the epithelial cells and the culture duration had a profound effect on the susceptibility of airway epithelial cells to SARS-CoV-2 infection.

Time of Culturing Affects the Proportion of Cell Types Related to MCC

Since we found increased viral infection upon prolonged differentiation time and additionally, we observed that SARS-CoV-2 infection targets mostly ciliated cells, goblet cells, and transient secretory cells (which we also confirmed for ALI-PTEC [online suppl. Fig. S3c]), we hypothesized that the numbers of these target cells changed over time of differentiation. We compared cellular composition between 3-, 4-, and 5-week-differentiated cultures and found that these cultures at all time points expressed markers related to all dominant epithelial cell types (ciliated, goblet, club, and basal cells) in ALI-PBEC and PTEC (online suppl. Fig. S3b). However, there were clear differences in the proportions of goblet and ciliated cells over time of differentiation (Fig. 3d). Using FOXJ1 and acetylated α-tubulin as markers for ciliated cells, we observed that the percentage of $FOXJ1^+$ cells was significantly higher in ALI-PBEC after 5-week culture compared to 3-week cultures. Also, the percentage of ciliated cells was significantly higher in ALI-PBEC than in ALI-PTEC at all culture durations (Fig. 3e). The change in the percentage of $MUC5AC^+$ goblet cells was not significant over time in ALI-PBEC and ALI-PTEC (Fig. 3e). Additionally, the number of transient secretory cells was higher in ALI-PBEC than in ALI-PTEC (Fig. 3e). Furthermore, mRNA levels of *FOXJ1* were significantly increased in 4-week ALI-PBEC compared to 3-week cultures; however, they did not further increase in 5-week cultures (online suppl. Fig. S3d). In addition, *FOXJ1* mRNA was higher in 4/5-week ALI-PBEC cultures compared to 4/5-week PTEC cultures (online suppl. Fig. S3d).

Fig. 2. Effect of IL-13 treatment and DAPT-mediated inhibition of Notch signaling on epithelial susceptibility to SARS-CoV-2 infection. ALI-PBEC (mix of 4–5 donors) were differentiated for 3 weeks before addition of DAPT (5 μM) or IL-13 (1 ng/mL) and differentiation for an additional 2 weeks. **a** After in total 5 weeks of differentiation, ALI-PBEC were fixed, stained using primary antibodies against MUC5AC and FOXJ1 (goblet cell marker, ciliated cell marker) or acetylated α-tubulin together with FOXJ1 (ciliated cell markers) in combination with DAPI for nuclear staining, analyzed by immunofluorescence microscopy, and quantified by ImageJ. Immunofluorescence images shown are representative merged z-stack images for results of 3 independent experiments with ×400 original magnification. **b** SARS-CoV-2 infected cells were stained with primary antibodies against SARS-CoV-2 N protein (JUC3) in combination with DAPI for nuclear staining. Immunofluorescence images shown are representative merged z-stack images for results of 3 independent experiments with ×400 original magnification. **c** Intracellular viral RNA copies were measured by RT-qPCR. **d** Plaque assay was performed to titrate viral progeny in the apical washes. $n = 3$ independent experiments derived from 3 different donor mixes. Data are mean ± SEM. Analysis of differences was conducted using two-way ANOVA with a Tukey's/Bonferroni post hoc test. Significant differences are indicated by $*p < 0.05$ compared with untreated samples. **e** Immunostaining of control, DAPT- or IL-13-treated cultures at 72 hpi with antibodies against MUC5AC (goblet cell marker), FOXJ1 (ciliated cell marker), and SARS-CoV-2 N protein in combination with DAPI for nuclear staining. Immunofluorescence images shown are representative merged z-stack images for results of 3 independent experiments with ×400 original magnification.

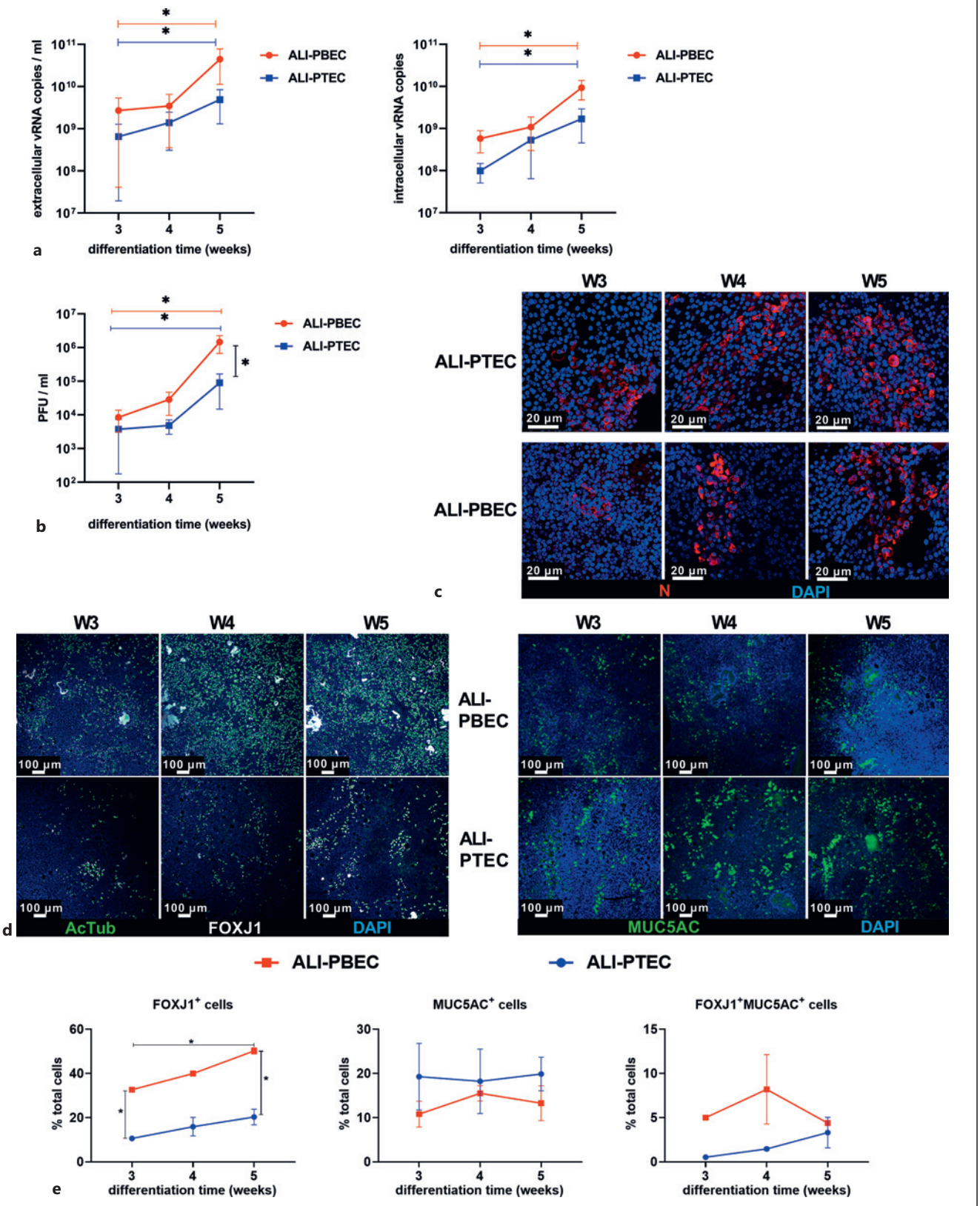

3

(For legend see next page.)

MUC5AC mRNA levels were higher at week 5 in ALI-PTEC cultures compared to week 3 and also higher than in week 5 ALI-PBEC (online suppl. Fig. S3d). In contrast, there was no significant difference in the expression of *SCGB1A1* (club cell marker) and *TP63* (basal cell marker) (online suppl. Fig. S3d). These results suggest that despite the early presence of transcripts which are specific for certain cell types, differentiation of certain cell types (which also requires expression at the protein level) continues for several weeks in cultures at ALI. Altogether, we found differences in the percentage of ciliated cells between PTEC and PBEC and between cultures that differed in their incubation time at ALI, which was in line with differences in viral load.

Changes in Gene Expression Associated with SARS-CoV-2 Target Cells

To further explore the gradual increase in susceptibility to SARS-CoV-2 infection with longer culture time, we compared the expression profiles of 3-week and 5-week uninfected differentiated cultures by bulk RNA-Seq and applied cellular deconvolution. We identified 169 DEGs, of which expression of 49 genes was upregulated, while expression of 120 genes was downregulated in ALI-PBEC at 5 versus 3 weeks (Fig. 4a; online suppl. Table S1). In ALI-PTEC, the expression of 32 genes increased, and 26 genes showed decreased expression in 5-week cultures compared to 3-week cultures (Fig. 4b; online suppl. Table S1). Gene set enrichment analysis was conducted to identify the top differentially upregulated and downregulated gene sets in ALI-PBEC between week 5 and week 3 (Table 2). A striking difference in ALI-PBEC between week 5 and week 3 was observed for the gene sets related to markers of ciliated and basal cells. Cellular deconvolution analysis further showed that the relative proportion of ciliated cells was increased in 5-week ALI-PBEC cultures, and the same trend was also found for ALI-PTEC (Fig. 4c, d). Altogether, RNA-Seq analysis did not reveal additional changes in cell types between the 3- and 5-week culture duration.

Cell Culture Duration Alters Expression of SARS-CoV-2 Entry Factors

The expression of host proteins that have been linked to entry of SARS-CoV-2 varies between the different airway epithelial cell types [23]. Therefore, we investigated whether the observed increase in susceptibility to SARS-CoV-2 with increased differentiation time and the effect of the anatomical origin was related to the expression of the main receptor ACE2 or other factors involved in entry. We compared the mRNA levels of different viral entry factors between the single-donor cultures that displayed the highest and lowest viral loads (Fig. 1a, 5a). Interestingly, the culture with the highest viral load expressed higher mRNA levels of *CTSL* and *TMPRSS2* at baseline, while other factors did not differ. Furthermore, we assessed the expression of cell entry factors in cultures of varying differentiation time using our RNA-Seq dataset (Fig. 5b). In both ALI-PBEC and ALI-PTEC cultures, there was a significant increase in expression of *TMPRSS2* in 5-week cultures compared to 3-week cultures. In addition, expression of *CTSL* was significantly increased, while expression of *CD147* was decreased at 5 weeks compared to 3 weeks in ALI-PBEC. However, expression of *NRP1* was reduced at 5 weeks compared to 3 weeks in ALI-PTEC, and expression of *ACE2*, *FURIN*, and *NRP1* was lower in 3-week ALI-PBEC compared to 3-week ALI-PTEC (Fig. 5b). We compared the expression of these genes by RT-qPCR in 3- and 5-week cultures and also included 4-week cultures (online suppl. Fig. S4a). With longer culture duration, in both ALI-PBEC and ALI-PTEC, gene expression of *CTSL* and *TMPRSS2* indeed increased over time, and a significant increase was found in expression of *TMPRSS2* in 4-week ALI-PBEC compared to 3-week cultures. Gene expression of *ACE2* and *GRP78* did not change with culture duration. A significant increase in expression of *CD147*

Fig. 3. Effect of culture duration on SARS-CoV-2 infection in PTEC and PBEC. ALI-PBEC/ALI-PTEC (mix of 5 donors) cultured for 3–5 weeks were infected with SARS-CoV-2 (30,000 PFU per insert). **a** Extracellular viral RNA copies in the apical wash or intracellular copies were measured by RT-qPCR. **b** Viral infectious progeny was quantified by plaque assay in Vero E6 cells. Mean values ± SEM from 3 independent experiments using 3 different donor mixes are shown. Statistical analysis was conducted using two-way ANOVA with a Tukey's/Bonferroni post hoc test. Significant differences are indicated by $*p < 0.05$. **c** Cells were stained for immunofluorescence microscopy with rabbit polyclonal anti-SARS-CoV-2 N protein antibody (JUC3) and DAPI for nuclear staining. Images shown are representative merged z-stack images for results obtained with ALI-PBEC and ALI-PTEC from the same 3 independent experiments shown in (**a**, **b**) at ×400 original magnification. **d** Immunofluorescence staining of 3-, 4-, 5-week cultures using antibodies against acetylated α-tubulin and FOXJ1 (ciliated cell markers) or MUC5AC (goblet cell marker) in combination with DAPI for nuclear staining. Images shown are representative merged z-stack images for results of 3 independent experiments with ×100 original magnification. **e** Quantification of $FOXJ^+$, $MUC5AC^+$ cells and $FOXJ1^+MUC5AC^+$ cells was done by ImageJ software.

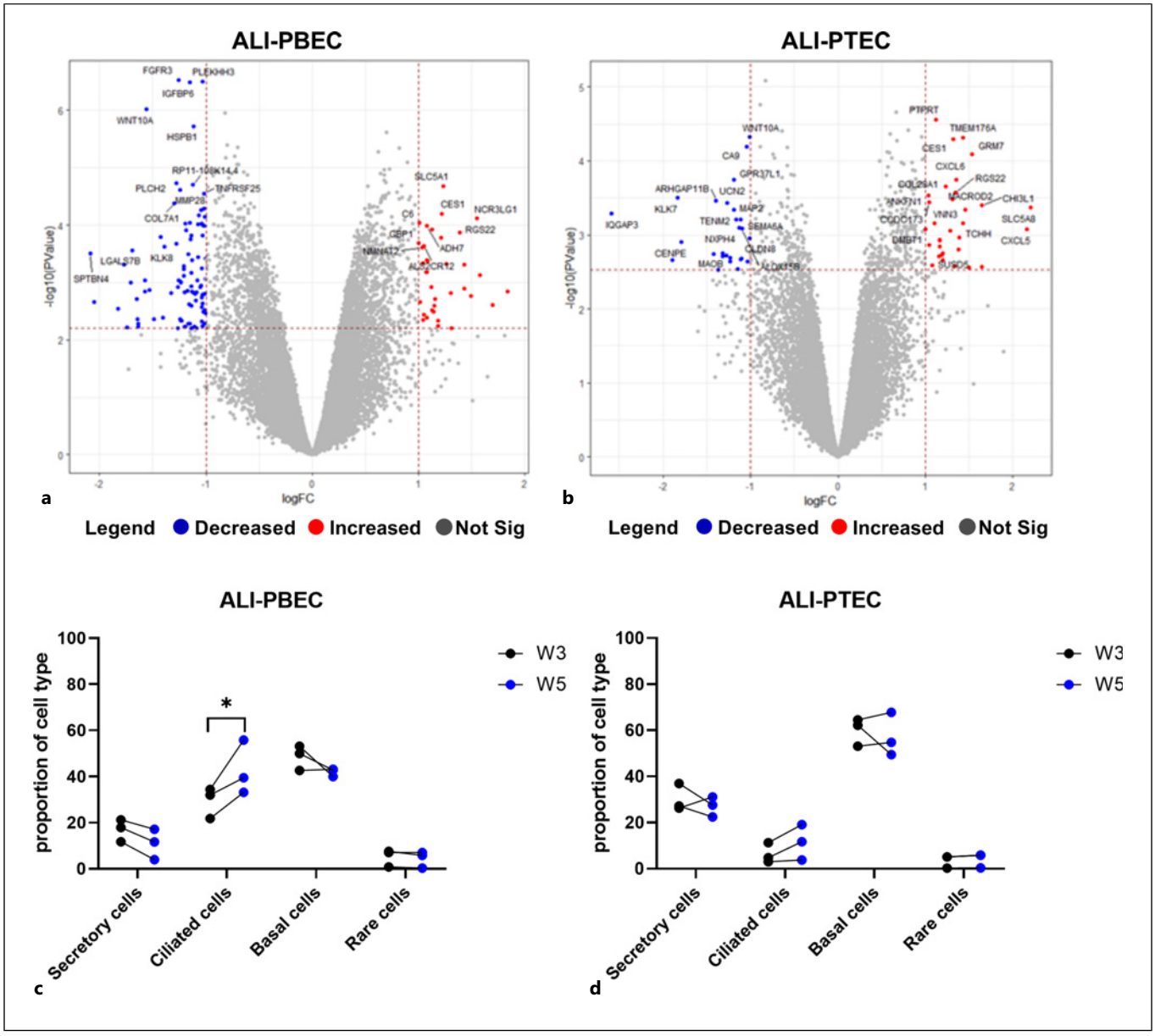

Fig. 4. Transcriptional responses comparing 3- and 5-week-differentiated primary bronchial and tracheal cells using RNA-Seq analysis. PBEC and PTEC were cultured at ALI for 3 weeks or 5 weeks. RNA was isolated from these samples and used for RNA-Seq analysis. **a**, **b** Volcano plots depicting changes in the gene expression profiles of 5-week cultures compared to 3-week cultures from ALI-PBEC or ALI-PTEC. The DEGs were considered significant when they had a Benjamini-Hochberg *p* value <0.1 and a fold change >2. Genes depicted in red are significantly upregulated, while genes depicted in blue are significantly downregulated in 5-week cultures compared to 3-week cultures in ALI-PBEC (**a**) or ALI-PTEC (**b**). **c**, **d** Relative proportion of different cell types for each donor mix in ALI-PBEC (**c**) cultures and ALI-PTEC (**d**) cultures as determined by cellular deconvolution of the transcriptomic datasets.

was observed in 4-week ALI-PBEC compared to 3-week cultures (online suppl. Fig. S4a). Treatment with DAPT or IL-13 did not affect expression of SARS-CoV-2 entry factors (online suppl. Fig. S4b). These findings indicated that changes in expression of *CTSL* and *TMPRSS2* could (in part) be responsible for the observed differences in susceptibility to SARS-CoV-2 infection between 3-, 4-, and 5-week differentiated cultures.

J Innate Immun 2023;15:562–580
DOI: 10.1159/000530374

Table 2. Top gene sets of the differentially expressed genes analyzed using gene set enrichment analysis (GSEA)

Direction	Gene set name	Genes in gene set (*K*), *n*	Description	Genes in overlap (*k*), *n*	*k*/*K*	*p* value	FDR *q* value
Upregulated	MURARO_PANCREAS_DUCTAL_CELL	1,276		12	0.0094	9.25E−9	1.79E−4
Upregulated	GOBP_DEFENSE_RESPONSE	1,739	Reactions, triggered in response to the presence of a foreign body or the occurrence of an injury, which result in restriction of damage to the organism attacked or prevention/recovery from the infection caused by the attack [GOC:go_curators]	12	0.0069	2.7E−7	2.3E−3
Upregulated	WP_PROXIMAL_TUBULE_TRANSPORT	58	Proximal tubule transport	4	0.0690	5.25E−7	2.3E−3
Upregulated	WP_NRF2_PATHWAY	145	NRF2 pathway	5	0.0345	5.77E−7	2.3E−3
Upregulated	DESCARTES_FETAL_INTESTINE_INTESTINAL_EPITHELIAL_CELLS	276	descartes DE_gene_by_organ.csv, fold change >5, *q* value <0.05, *p* value <0.05	6	0.0217	5.94E−7	2.3E−3
Upregulated	REACTOME_G_ALPHA_I_SIGNALLING_EVENTS	314	G alpha (i) signalling events	6	0.0191	1.26E−6	3.46E−3
Upregulated	GOMF_SOLUTE_SODIUM_SYMPORTER_ACTIVITY	72	Enables the transfer of a solute or solutes from one side of a membrane to the other according to the reaction: solute (out) + Na + (out) = solute (in) + Na+ (in) [GOC:ai]	4	0.0556	1.26E−6	3.46E−3
Upregulated	WP_NUCLEAR_RECEPTORS_METAPATHWAY	321	Nuclear receptors meta-pathway	6	0.0187	1.43E−6	3.46E−3
Upregulated	TRAVAGLINI_LUNG_CILIATED_CELL	1,094		9	0.0082	2.59E−6	5.57E−3
Upregulated	TRAVAGLINI_LUNG_MACROPHAGE_CELL	201		5	0.0249	2.88E−6	5.58E−3
Downregulated	GOCC_SUPRAMOLECULAR_COMPLEX	1,329	A cellular component that consists of an indeterminate number of proteins or macromolecular complexes organized into a regular, higher-order structure such as a polymer, sheet, network, or fiber. [GOC:dos]	18	0.0135	9.81E−9	8.53E−5
Downregulated	TRAVAGLINI_LUNG_PROLIFERATING_BASAL_CELL	891		15	0.0168	1.12E−8	8.53E−5
Downregulated	HAY_BONE_MARROW_STROMAL	767		14	0.0183	1.32E−8	8.53E−5
Downregulated	TRAVAGLINI_LUNG_BASAL_CELL	188		8	0.0426	3.6E−8	1.61E−4
Downregulated	GOCC_SUPRAMOLECULAR_POLYMER	996	A polymeric supramolecular structure [GOC:dos]	15	0.0151	4.84E−8	1.61E−4

Table 2 (continued)

Direction	Gene set name	Genes in gene set (*K*), *n*	Description	Genes in overlap (*k*), *n*	*k*/*K*	*p* value	FDR *q* value
Downregulated	ZHONG_PFC_C2_UNKNOWN_NPC	76		6	0.0789	5.04E−8	1.61E−4
Downregulated	HALLMARK_KRAS_SIGNALING_DN	200	Genes downregulated by KRAS activation	8	0.0400	5.81E−8	1.61E−4
Downregulated	NABA_MATRISOME	1,026	Ensemble of genes encoding extracellular matrix and extracellular matrix-associated proteins	15	0.0146	7.1E−8	1.72E−4
Downregulated	MANNO_MIDBRAIN_NEUROTYPES_HNPROG	229	Cell types are named using anatomical and functional mnemonics prefixed by "m" or "h" to indicate mouse and human, respectively: OMTN, oculomotor, and trochlear nucleus; Sert, serotonergic; NbM, medial neuroblast; NbDA, neuroblast dopaminergic; DA0-2, dopaminergic neurons; RN, red nucleus; Gaba1-2, GABAergic neurons; mNbL1-2, lateral neuroblasts; NbML1-5, mediolateral neuroblasts; NProg, neuronal progenitor; Prog, progenitor medial floorplate (FPM), lateral floorplate (FPL), midline (M), basal plate (BP); Rgl1-3, radial glia-like cells; Mgl, microglia; Endo, endothelial cells; Peric, pericytes; Epend, ependymal; OPC, oligodendrocyte precursor cells	8	0.0349	1.64E−7	3.45E−4
Downregulated	FAN_EMBRYONIC_CTX_MICROGLIA_1	155		7	0.0452	1.78E−7	3.45E−4

p value was calculated from the hypergeometric distribution for (*k*−1, *K*, *N*−*K*, *n*) where *k* is the number of genes in the intersection of the query set with a set from MSigDB; *K* is the number of genes in the set from MSigDB; *N* is the total number of gene universe (all known human gene symbols); and *n* is the number of genes in the query set. FDR *q* value means the false discovery rate analog of hypergeometric *p* value after correction for multiple hypotheses.

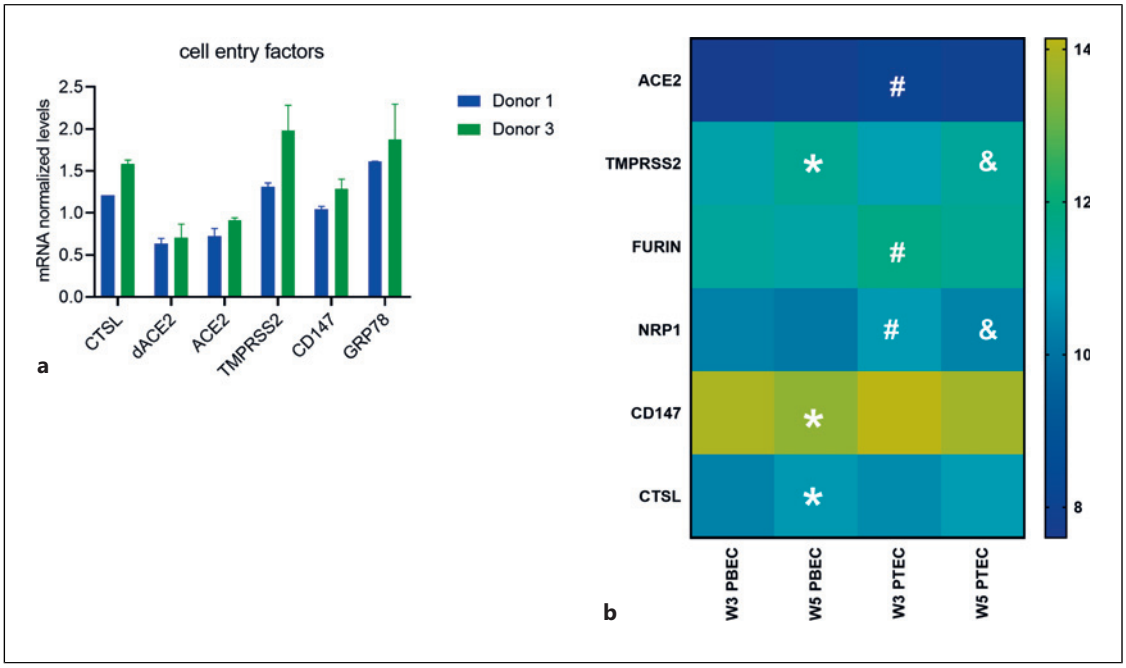

Fig. 5. Effect of donor variation and culture duration on expression of SARS-CoV-2 cell entry factors. **a** RT-qPCR analysis of gene expression of viral cell entry factors in two single-donor cultures at 5 weeks. Data are mean values ± SEM. $n = 2$ duplicated wells per donor. **b** Heatmap of transcriptional changes (RNA-Seq data) of SARS-CoV-2 cell entry factors in 3-week and 5-week PBEC and PTEC. Differences were assessed by a two-way ANOVA with Tukey's test, and the significant differences were considered at $p < 0.05$. * = 5-week ALI-PBEC versus 3-week ALI-PBEC; & = 5-week ALI-PTEC versus 3-week ALI-PTEC; # = 3-week ALI-PTEC versus 3-week ALI-PBEC.

Cell Culture Duration Does Not Affect SARS-CoV-2-Induced Antiviral Responses

Antiviral responses in the epithelium are critical for protection against viral infections. Therefore, we investigated whether antiviral responses changed depending on the ALI culture duration and whether this could provide an additional explanation of the observed increased susceptibility to infection with longer culture times. In ALI-PTEC, SARS-CoV-2-induced mRNA levels of both *IFNB1* and *IFNL1* increased significantly with culture duration. When cultures were infected at weeks 3 or 4, there was little *IFNB1* or *IFNL1* mRNA produced, while expression of these genes was strongly upregulated by SARS-CoV-2 infection in 5-week-old cultures (online suppl. Fig. S5a, b). Gene expression analysis of *IFNB1* and *IFNL1* showed a similar increasing trend in ALI-PBEC upon infection (online suppl. Fig. S5c, d). When 5-week PBEC were (long-term) treated with DAPT, we observed lower SARS-CoV-2-induced antiviral responses than in untreated and IL-13-treated cultures (online suppl. Fig. S5e, f). All these findings correlate with the observed differences in the number of infected cells and viral load resulting from culture duration and DAPT and IL-13 treatment (Fig. 2). This suggests that antiviral responses were not affected by differentiation time or long-term DAPT/IL-13 treatment but rather differed as a direct consequence of differences in the level of infection.

Discussion

Here, we investigated the influence of cellular composition and differentiation of human primary airway epithelial cell cultures on SARS-CoV-2 infection biology. Our key finding is that changes in cell types related to MCC, i.e., ciliated and goblet cells, influence SARS-CoV-2 infection of human primary airway epithelial cells. Specifically, a higher percentage of ciliated cells appears to be the main contributing factor to a higher level of infection. This is likely a consequence of their higher susceptibility to infection in comparison to the other cell types and possibly their contribution to spreading of virus across the epithelial surface of the culture. Nevertheless, our data also suggest that the presence of mucus and/or goblet cells is important since a reduction in goblet cells reduced the viral load, even

in cultures with a higher percentage of ciliated cells. Finally, we provide experimental evidence for infection of transient secretory cells by SARS-CoV-2.

With regard to differentiation time, there is no golden standard protocol for ALI-primary airway epithelial cell cultures to obtain cultures that best resemble the human epithelial cellular composition. The literature reports that differentiation times anywhere between 2 and 6 weeks after start of ALI culture are needed to have all key cell types present in culture [18, 19, 44].

In line with a recent study investigating SARS-CoV-2 infection using primary airway epithelial cells [19], and based on our own study comparing 3- to 5-week-old cultures, we decided to use 5-week-differentiated ALI-PBEC cultures. We found a reproducible increase in viral titers over time post infection. In addition, cultures of well-differentiated airway epithelial cells adequately model in vivo host antiviral responses [45, 46], which we could confirm also for SARS-CoV-2 infection by detecting increased mRNA levels of *IL-6* and *CXCL8*. In contrast, downregulated expression of *IL-6* and *CXCL8* was reported in the human bronchial epithelial cell line 16HBE [47].

We confirmed that both ciliated and goblet cells were infected by SARS-CoV-2 in our ALI cultures, whereas no infected club and basal cells were detected (data not shown). This is consistent with results from recent studies looking into the cellular tropism of SARS-CoV-2, showing infection of multiple epithelial cell types, among them ciliated cells, goblet cells, and club cells of the airway epithelium and type 2 alveolar epithelial cells [18, 19, 48, 49]. Additionally, we also observed cells co-expressing markers of ciliated cells (FOXJ1) and goblet cells (MUC5AC) in our cultures. This specific cell population, which was recently reported by, e.g., Ruiz Garcia et al. [50] and by Vieira Braga et al. [51], is suggested to represent a transitional state between goblet and ciliated cells and was recently labeled as transient secretory cells [25]. Based on their relatively high co-expression of ACE2 and TMPRSS2, Lukassen et al. [25] suggested that these transient secretory cells may be particularly vulnerable to SARS-CoV-2 infection. Although we showed for the first time that SARS-CoV-2 was also able to infect these cells, it remains unknown if the low percentage of these cells in our culture model significantly contributed to the overall level of infection. Considering the role in MCC of ciliated, goblet, and potentially transient secretory cells, we conclude that cells involved in MCC are predominantly infected by SARS-CoV-2.

To investigate the role of cellular composition in susceptibility to viral infection, we skewed cell differentiation with the Notch signaling inhibitor DAPT [43], which resulted in cultures that constituted a high number of ciliated cells but lacked goblet cells and transient secretory cells. Surprisingly, the viral load in these cultures was reduced compared to untreated cultures. A possible explanation would be that ciliated cells become infected by the virus, and mucus produced by goblet cells helps spread the infection after release, which would be consistent with previous findings that SARS-CoV-2 infects ciliated cells with attached mucus [52]. Conversely, the modulation with IL-13 (slightly) increased viral loads compared to control and DAPT-treated cultures, which is in line with the suggestion from other studies that patients with allergic asthma, a disease associated with IL-13-induced changes in epithelial cell composition, may be somewhat more susceptible to SARS-CoV-2 infection [53]. Others have observed that treatment with IL-13 reduced viral RNA copies in ALI-cultured airway epithelial cells [54, 55]. There is no clear explanation for this discrepancy, although the reduced levels of *ACE2* after IL-13 treatments that were found in these studies might have been responsible for the reduced infection levels. However, in our studies, ACE2 expression was not affected by IL-13 treatment. Furthermore, we used a much lower MOI (0.03 vs. 0.5), and therefore, even if IL-13 reduces the number of the main target cells (e.g., ciliated cells), this is not expected to have much effect in our setup because the amount of susceptible cells will likely not be limiting due to the low MOI. Collectively, our observations indicate that DAPT- and IL-13-mediated modulation of epithelial cell differentiation does not provide a simple link between differences in epithelial cell composition and susceptibility to SARS-CoV-2 infection. A combination of factors appears to play a role. For example, mucus secretion by goblet cells [56], when excessive, could hinder clearance of the virus in the epithelium. We therefore used additional approaches to study the contributing effect of cellular composition to SARS-CoV-2 infection. We could demonstrate that changes in cellular composition either linked to anatomical origin, donor, or culture time influenced SARS-CoV-2 infection. The shared outcome was that for each variable, the number of target cells correlated to the viral load, suggesting that the percentage of ciliated cells is a strong contributing factor to the SARS-CoV-2 infection rate.

Considering that expression of viral entry factors varies between different cell types, we furthermore investigated their expression in cells from different donors, the effect of culture duration, and the impact of treatment with DAPT and IL-13. According to the literature, all main cell types express *TMPRSS2,* and the highest expression is found in transient secretory cells [25]. *CTSL* gene expression was reported to be higher in ciliated cells compared to other epithelial cell types [57]. When we compared two single

donors, cell cultures isolated from one donor expressed more *CTSL* and *TMPRSS2,* which was in line with the observed higher viral replication and higher abundance of ciliated cells in this donor. In our study, an increased expression of *CTSL* as well as *TMPRSS2* was also found with prolonged culture duration. Thus, the difference in *CTSL* expression could link to changes in the ciliated cell number, which supports the role of ciliated cells in viral replication. Furthermore, in line with this, CTSL levels were recently found to be positively correlated with severity of disease in COVID-19 patients, pointing to its role in enhancement of infection [58]. Other studies evaluated the role of CTSL and TMPRSS2 in SARS-CoV-2 infection by using E64d (an inhibitor of cysteine proteases, including CTSL) and camostat mesylate (an inhibitor of serine proteases, including TMPRSS2) [22, 59]. It was shown that both E64d and camostat mesylate inhibited infection by Wuhan, Delta, and Omicron isolates, confirming the role of CTSL and TMPRSS2 in viral entry.

We excluded possible effects of changes in antiviral responses on the gradual increase in viral infection with the prolonged culture duration since we did not observe lower expression of type I and III IFNs over culture time at ALI but rather found a correlation with the level of viral replication. Our study demonstrates that the use of mixed donor cultures is an efficient way to recapitulate natural variability between donors while saving on resources (cells, culture plastics, and media) that can be in high demand/short supply during pandemics. The level of donor-to-donor variation was also represented in inter-experimental variation when using the same donor mix. Inevitably, our study has some limitations. First, it needs to be noted that the comparison between PBEC and PTEC in this study should be interpreted with caution because PBEC were derived from tumor-free resected bronchial tissue from (ex-)smoking patients with lung cancer and PTEC were from donor lungs without lung disease. Second, the fact that we used an early pandemic SARS-CoV-2 strain in our studies could be considered a limitation, but this variant is still widely used as the model in (fundamental) studies on virus replication and antivirals. Studying this virus is still important to increase our preparedness for future outbreaks of highly pathogenic zoonotic coronaviruses. Several other studies have already compared the replication of different viruses, including recent omicron variants in human airway epithelial cell cultures [59–61]. It would be interesting to investigate if variants like alpha or delta, which have been reported to have a replicative advantage in human airway epithelial cell cultures, are likewise impacted by the changes in differentiated cultures that we observed in this study. Finally, we used cultures containing only epithelial cells. Adding immune cells to the culture system could offer interesting possibilities for future studies to investigate their impact on host responses during infection.

Overall, in this study, we have established that epithelial cell types related to MCC (i.e., ciliated, goblet, and transient secretory cells) seem pivotal for SARS-CoV-2 infection and spread of the infection over the epithelial tissue. This study underlines the importance of assessing these cell types and the role of mucus when studying how SARS-CoV-2 infection biology is affected in patients with chronic lung disease, such as those with chronic type 2 inflammation in asthma or in chronic obstructive pulmonary disease, where epithelial remodeling likely has shifted these cell type ratios.

Statement of Ethics

Patients from which this PBEC were derived were enrolled in the biobank via a no-objection system for coded anonymous further use of such tissue (www.coreon.org). However, since January 9, 2022, patients have been enrolled in the biobank using active informed consent in accordance with local regulations from the LUMC Biobank with approval by the Institutional Medical Ethical Committee (B20.042/Ab/ab and B20.042/Kb/kb). For the present study, cells from patients were used that were collected before January 9, 2022, and based on the regulations of the no-objection system, individual informed consent was not needed. PTEC were isolated from residual tracheal and main stem bronchial tissue from lung transplant donors postmortem at the University Medical Center Essen (Essen, Germany). Use of such donor tissue for research was approved by the Ethical Committee of the medical faculty of the University of Duisburg-Essen (ID: 19-8717-BO). Written informed consent for the use of PTEC was provided by the transplant recipients of the respective lungs. A preprint version of this article is available on bioRxiv [62].

Conflict of Interest Statement

The authors have no conflicts of interest to declare.

Funding Sources

This study was supported by a COVID-19 MKMD grant from The Netherlands Organization for Health Research and Development (ZonMw) and the Dutch Society for the Replacement of Animal Testing (Stichting Proefdiervrij) (Grant #114025007). C.S.-B. was supported by the Coordination for the Improvement of Higher Education Personnel (CAPES) (process no. 88881.171440/2018-01), Ministry of Education, Brazil. Part of this research was supported by the Leiden University Fund (LUF), the Bontius Foundation, and donations from the crowdfunding initiative "wake up to corona." This study has also received

funding from the European Union's Horizon 2020 research and innovation program under Grant No. 10100362 (the SCORE project). Part of RNA-Seq and analysis was supported by a RSEOH-CAG Rapid Response Research Initiative and a RSEOH-CAG 2021 Extension Grant. Collection of primary human tracheal epithelial cells was supported by grants from the Deutsche Forschungsgemeinschaft (DFG) (Ta 275/7-1 and Ta 275/8-1) to C.T.

Author Contributions

Melissa Thaler, Ying Wang, Anne M. van der Does, Peter J. Bredenbeek, Pieter S. Hiemstra, and Martijn J. van Hemert were involved in study design and conceptualization. Melissa Thaler, Ying Wang, Dennis K. Ninaber, Natacha S. Ogando, and Clarisse Salgado-Benvindo performed experiments. Alen Faiz performed RNA-Seq analysis and cellular deconvolution. Hendrik Beckert and Christian Taube collected and isolated human tracheal epithelial cells. Melissa Thaler and Ying Wang wrote the manuscript. Anne M. van der Does, Pieter S. Hiemstra, Martijn J. van Hemert, Eric J. Snijder, and Peter J. Bredenbeek revised the manuscript. The final version was critically reviewed and approved by all the authors.

Data Availability Statement

The RNA-Seq data that support the findings of this study will be openly available in the repository European Genome-Phenome Archive (EGA). Until then, all data are available upon reasonable request by contacting the corresponding author. All other data generated or analyzed during this study are included in this article and its online supplementary material.

References

1 Chakraborty I, Maity P. COVID-19 outbreak: migration, effects on society, global environment and prevention. Sci Total Environ. 2020 Aug 1;728:138882.
2 Toyoshima Y, Nemoto K, Matsumoto S, Nakamura Y, Kiyotani K. SARS-CoV-2 genomic variations associated with mortality rate of COVID-19. J Hum Genet. 2020 Dec;65(12):1075–82.
3 Yurkovetskiy L, Wang X, Pascal KE, Tomkins-Tinch C, Nyalile TP, Wang Y, et al. Structural and functional analysis of the D614G SARS-CoV-2 spike protein variant. Cell. 2020 Oct 29;183(3):739–51.e8.
4 Trevisan C, Noale M, Prinelli F, Maggi S, Sojic A, Di Bari M, et al. Age-related changes in clinical presentation of covid-19: the EPICOVID19 web-based survey. Eur J Intern Med. 2021;86:41–7.
5 Alwani M, Yassin A, Al-Zoubi RM, Aboumarzouk OM, Nettleship J, Kelly D, et al. Sex-based differences in severity and mortality in COVID-19. Rev Med Virol. 2021 Nov;31(6):e2223.
6 Yu W, Rohli KE, Yang S, Jia P. Impact of obesity on COVID-19 patients. J Diabetes Complications. 2021 Mar;35(3):107817.
7 Carraturo F, Del Giudice C, Morelli M, Cerullo V, Libralato G, Galdiero E, et al. Persistence of SARS-CoV-2 in the environment and COVID-19 transmission risk from environmental matrices and surfaces. Environ Pollut. 2020 Oct;265(Pt B):115010.
8 Bansal M. Cardiovascular disease and COVID-19. Diabetes Metab Syndr. 2020 May–Jun;14(3):247–50.
9 Ovsyannikova IG, Haralambieva IH, Crooke SN, Poland GA, Kennedy RB. The role of host genetics in the immune response to SARS-CoV-2 and COVID-19 susceptibility and severity. Immunol Rev. 2020;296(1):205–19.
10 Park SE. Epidemiology, virology, and clinical features of severe acute respiratory syndrome -coronavirus-2 (SARS-CoV-2; Coronavirus Disease-19). Clin Exp Pediatr. 2020;63(4):119–24.
11 Zhou P, Yang X-L, Wang X-G, Hu B, Zhang L, Zhang W, et al. A pneumonia outbreak associated with a new coronavirus of probable bat origin. Nature. 2020;579(7798):270–3.
12 Hiemstra PS, McCray PB Jr, Bals R. The innate immune function of airway epithelial cells in inflammatory lung disease. Eur Respir J. 2015 Apr;45(4):1150–62.
13 Iwasaki A, Foxman EF, Molony RD. Early local immune defences in the respiratory tract. Nat Rev Immunol. 2017 Jan;17(1):7–20.
14 Bovard D, Giralt A, Trivedi K, Neau L, Kanellos P, Iskandar A, et al. Comparison of the basic morphology and function of 3D lung epithelial cultures derived from several donors. Curr Res Toxicol. 2020 Jun 10;1:56–69.
15 Belgacemi R, Luczka E, Ancel J, Diabasana Z, Perotin JM, Germain A, et al. Airway epithelial cell differentiation relies on deficient Hedgehog signalling in COPD. EBioMedicine. 2020 Jan;51:102572.
16 Leung C, Wadsworth SJ, Yang SJ, Dorscheid DR. Structural and functional variations in human bronchial epithelial cells cultured in air-liquid interface using different growth media. Am J Physiol Lung Cell Mol Physiol. 2020 May 1;318(5):L1063–73.
17 Hou YJ, Okuda K, Edwards CE, Martinez DR, Asakura T, Dinnon KH 3rd, et al. SARS-CoV-2 reverse genetics reveals a variable infection gradient in the respiratory tract. Cell. 2020 Jul 23;182(2):429–46.e14.
18 Hao S, Ning K, Kuz CA, Vorhies K, Yan Z, Qiu J. Long-term modeling of SARS-CoV-2 infection of in vitro cultured polarized human airway epithelium. mBio. 2020 Nov 6;11(6):e02852–20.
19 Zhu N, Wang W, Liu Z, Liang C, Wang W, Ye F, et al. Morphogenesis and cytopathic effect of SARS-CoV-2 infection in human airway epithelial cells. Nat Commun. 2020 Aug 6;11(1):3910.
20 Ehre C. SARS-CoV-2 infection of airway cells. N Engl J Med. 2020 Sep 3;383(10):969.
21 Aguiar JA, Tremblay BJM, Mansfield MJ, Woody O, Lobb B, Banerjee A, et al. Gene expression and in situ protein profiling of candidate SARS-CoV-2 receptors in human airway epithelial cells and lung tissue. Eur Respir J. 2020 Sep;56(3):2001123.
22 Hoffmann M, Kleine-Weber H, Schroeder S, Krüger N, Herrler T, Erichsen S, et al. SARS-CoV-2 cell entry depends on ACE2 and TMPRSS2 and is blocked by a clinically proven protease inhibitor. Cell. 2020 Apr 16;181(2):271–80.e8.
23 Sungnak W, Huang N, Bécavin C, Berg M, Queen R, Litvinukova M, et al. SARS-CoV-2 entry factors are highly expressed in nasal epithelial cells together with innate immune genes. Nat Med. 2020 May;26(5):681–7.
24 Wang S, Qiu Z, Hou Y, Deng X, Xu W, Zheng T, et al. AXL is a candidate receptor for SARS-CoV-2 that promotes infection of pulmonary and bronchial epithelial cells. Cell Res. 2021;31(2):126–40.
25 Lukassen S, Chua RL, Trefzer T, Kahn NC, Schneider MA, Muley T, et al. SARS-CoV-2 receptor ACE2 and TMPRSS2 are primarily expressed in bronchial transient secretory cells. EMBO J. 2020 May 18;39(10):e105114.
26 Bridges JP, Vladar EK, Huang H, Mason RJ. Respiratory epithelial cell responses to SARS-CoV-2 in COVID-19. Thorax. 2022;77(2):203–9.

27 Schrumpf JA, Ninaber DK, van der Does AM, Hiemstra PS. TGF-β1 impairs vitamin D-induced and constitutive airway epithelial host defense mechanisms. J Innate Immun. 2020;12(1):74–89.
28 Wang Y, Ninaber DK, van Schadewijk A, Hiemstra PS. Tiotropium and fluticasone inhibit rhinovirus-induced mucin production via multiple mechanisms in differentiated airway epithelial cells. Front Cell Infect Microbiol. 2020;10:278.
29 Kovacikova K, Morren BM, Tas A, Albulescu IC, van Rijswijk R, Jarhad DB, et al. 6′-β-Fluoro-Homoaristeromycin and 6′-fluoro-homoneplanocin A are potent inhibitors of chikungunya virus replication through their direct effect on viral nonstructural protein 1. Antimicrob Agents Chemother. 2020 Mar 24;64(4):e02532–19.
30 Corman VM, Landt O, Kaiser M, Molenkamp R, Meijer A, Chu DK, et al. Detection of 2019 novel coronavirus (2019-nCoV) by real-time RT-PCR. Eurosurveillance. 2020 Jan;25(3).
31 de Wilde AH, Raj VS, Oudshoorn D, Bestebroer TM, van Nieuwkoop S, Limpens RWAL, et al. MERS-coronavirus replication induces severe in vitro cytopathology and is strongly inhibited by cyclosporin A or interferon-α treatment. J Gen Virol. 2013 Aug;94(Pt 8):1749–60.
32 Graham C, Seow J, Huettner I, Khan H, Kouphou N, Acors S, et al. Neutralization potency of monoclonal antibodies recognizing dominant and subdominant epitopes on SARS-CoV-2 Spike is impacted by the B.1.1.7 variant. Immunity. 2021;54(6):1276–89.e6.
33 Mootha VK, Lindgren CM, Eriksson K-F, Subramanian A, Sihag S, Lehar J, et al. PGC-1alpha-responsive genes involved in oxidative phosphorylation are coordinately downregulated in human diabetes. Nat Genet. 2003;34(3):267–73.
34 Subramanian A, Tamayo P, Mootha VK, Mukherjee S, Ebert BL, Gillette MA, et al. Gene set enrichment analysis: a knowledge-based approach for interpreting genome-wide expression profiles. Proc Natl Acad Sci U S A. 2005;102(43):15545–50.
35 Aliee H, Massip F, Qi C, Stella de Biase M, van Nijnatten JL, Kersten ETG, et al. Determinants of SARS-CoV-2 receptor gene expression in upper and lower airways. medRxiv. 2020 Sep 2.
36 Sikkema L, Strobl D, Zappia L, Madissoon E, Markov N, Zaragosi L, et al. An integrated cell atlas of the human lung in health and disease. bioRxiv. 2022.
37 Newman AM, Liu CL, Green MR, Gentles AJ, Feng W, Xu Y, et al. Robust enumeration of cell subsets from tissue expression profiles. Nat Methods. 2015 May;12(5):453–7.
38 Mulay A, Konda B, Garcia G Jr, Yao C, Beil S, Villalba JM, et al. SARS-CoV-2 infection of primary human lung epithelium for COVID-19 modeling and drug discovery. Cell Rep. 2021;35(5):109055–5.
39 Salgado-Benvindo C, Thaler M, Tas A, Ogando NS, Bredenbeek PJ, Ninaber DK, et al. Suramin inhibits SARS-CoV-2 infection in cell culture by interfering with early steps of the replication cycle. Antimicrob Agents Chemother. 2020 Jul 22;64(8):e00900–20.
40 Huang J, Hume AJ, Abo KM, Werder RB, Villacorta-Martin C, Alysandratos KD, et al. SARS-CoV-2 infection of pluripotent stem cell-derived human lung alveolar type 2 cells elicits a Rapid epithelial-intrinsic inflammatory response. Cell Stem Cell. 2020 Dec 3;27(6):962–73.e7.
41 Katsura H, Sontake V, Tata A, Kobayashi Y, Edwards CE, Heaton BE, et al. Human lung stem cell-based alveolospheres provide insights into SARS-CoV-2-mediated interferon responses and pneumocyte dysfunction. Cell Stem Cell. 2020 Dec 3;27(6):890–904.e8.
42 Mertens TCJ, van der Does AM, Kistemaker LE, Ninaber DK, Taube C, Hiemstra PS. Cigarette smoke differentially affects IL-13-induced gene expression in human airway epithelial cells. Physiol Rep. 2017 Jul;5(13):e13347.
43 Amatngalim GD, Schrumpf JA, Dishchekenian F, Mertens TCJ, Ninaber DK, van der Linden AC, et al. Aberrant epithelial differentiation by cigarette smoke dysregulates respiratory host defence. Eur Respir J. 2018 Apr;51(4):1701009.
44 Zhang H, Rostami MR, Leopold PL, Mezey JG, O'Beirne SL, Strulovici-Barel Y, et al. Expression of the SARS-CoV-2 ACE2 receptor in the human airway epithelium. Am J Respir Crit Care Med. 2020 Jul 15;202(2):219–29.
45 Lieberman NAP, Peddu V, Xie H, Shrestha L, Huang M-L, Mears MC, et al. In vivo antiviral host transcriptional response to SARS-CoV-2 by viral load, sex, and age. PLoS Biol. 2020;18(9):e3000849.
46 Vanderheiden A, Ralfs P, Chirkova T, Upadhyay AA, Zimmerman MG, Bedoya S, et al. Type I and type III interferons restrict SARS-CoV-2 infection of human airway epithelial cultures. J Virol. 2020;94(19):e00985–20.
47 Liao Y, Li X, Mou T, Zhou X, Li D, Wang L, et al. Distinct infection process of SARS-CoV-2 in human bronchial epithelial cell lines. J Med Virol. 2020 Nov;92(11):2830–8.
48 Bost P, Giladi A, Liu Y, Bendjelal Y, Xu G, David E, et al. Host-viral infection maps reveal signatures of severe COVID-19 patients. Cell. 2020;181(7):1475–88.e12.
49 Ziegler CGK, Allon SJ, Nyquist SK, Mbano IM, Miao VN, Tzouanas CN, et al. SARS-CoV-2 receptor ACE2 is an interferon-stimulated gene in human airway epithelial cells and is detected in specific cell subsets across tissues. Cell. 2020;181(5):1016–35.e19.
50 Ruiz García S, Deprez M, Lebrigand K, Cavard A, Paquet A, Arguel MJ, et al. Novel dynamics of human mucociliary differentiation revealed by single-cell RNA sequencing of nasal epithelial cultures. Development. 2019 Oct 23;146(20):dev177428.
51 Vieira Braga FA, Kar G, Berg M, Carpaij OA, Polanski K, Simon LM, et al. A cellular census of human lungs identifies novel cell states in health and in asthma. Nat Med. 2019;25(7):1153–63.
52 Kimura H, Francisco D, Conway M, Martinez FD, Vercelli D, Polverino F, et al. Type 2 inflammation modulates ACE2 and TMPRSS2 in airway epithelial cells. J Allergy Clin Immunol. 2020 Jul;146(1):80–8.e8.
53 Eger K, Bel EH. Asthma and COVID-19: do we finally have answers? Eur Respir J. 2021 Mar;57(3):2004451.
54 Bonser LR, Eckalbar WL, Rodriguez L, Shen J, Koh KD, Ghias K, et al. The type 2 asthma mediator IL-13 inhibits severe acute respiratory syndrome coronavirus 2 infection of bronchial epithelium. Am J Respir Cell Mol Biol. 2022;66(4):391–401.
55 Morrison CB, Edwards CE, Shaffer KM, Araba KC, Wykoff JA, Williams DR, et al. SARS-CoV-2 infection of airway cells causes intense viral and cell shedding, two spreading mechanisms affected by IL-13. Proc Natl Acad Sci U S A. 2022 Apr 19;119(16):e2119680119.
56 Liu Y, Lv J, Liu J, Li M, Xie J, Lv Q, et al. Mucus production stimulated by IFN-AhR signaling triggers hypoxia of COVID-19. Cell Res. 2020 Dec;30(12):1078–87.
57 Ravindra NG, Alfajaro MM, Gasque V, Huston NC, Wan H, Szigeti-Buck K, et al. Single-cell longitudinal analysis of SARS-CoV-2 infection in human airway epithelium identifies target cells, alterations in gene expression, and cell state changes. PLoS Biol. 2021 Mar;19(3):e3001143.
58 Zhao M-M, Yang W-L, Yang F-Y, Zhang L, Huang W-J, Hou W, et al. Cathepsin L plays a key role in SARS-CoV-2 infection in humans and humanized mice and is a promising target for new drug development. Signal Transduct Target Ther. 2021;6(1):134.
59 Hui KPY, Ho JCW, Cheung MC, Ng KC, Ching RHH, Lai KL, et al. SARS-CoV-2 Omicron variant replication in human bronchus and lung ex vivo. Nature. 2022 Mar;603(7902):715–20.
60 Liu Y, Liu J, Johnson BA, Xia H, Ku Z, Schindewolf C, et al. Delta spike P681R mutation enhances SARS-CoV-2 fitness over Alpha variant. Cell Rep. 2022;39(7):110829.
61 Mache C, Schulze J, Holland G, Bourquain D, Gensch J-M, Oh D-Y, et al. SARS-CoV-2 Omicron variant is attenuated for replication in a polarized human lung epithelial cell model. Commun Biol. 2022;5(1):1138.
62 Wang Y, Thaler M, Ninaber DK, van der Does AM, Ogando NS, Beckert H, et al. Impact of human airway epithelial cellular composition on SARS-CoV-2 infection biology. bioRxiv. 2021.